The effects of theoretical formalism and data selection scheme on mantle models derived from waveform tomography

by

Charles Mégnin

and

Barbara Romanowicz

Berkeley Seismological Laboratory

and

Department of Geology & Geophysics

University of California

Berkeley, California 94720

Geophysical Journal International, in press

March 4, 1999

Abstract

Most global tomographic models to date are derived using a combination of surface wave (or normal mode) data and body wave travel time data. The travel time approach limits the number of phases available for inversion by requiring them to be isolated on the seismogram. This may ultimately result in limiting the resolution of 3D structure, at least in some depth ranges in the mantle. In previous work, we successfully derived a degree 12 whole mantle SH velocity tomographic model (SAW12D) using exclusively waveform data. In that inversion, a normal mode formalism suitable for body waveforms, the nonlinear asymptotic coupling theory (*NACT*), was combined with a bodywave windowing scheme, referred to as the 'individual wavepacket' (*IW*) technique, which allows to assign individual weights to different body-wave energy packets. We here compare the relative merits of this choice of theoretical formalism and windowing scheme, in different depth ranges in the mantle. Choosing as reference a model obtained using 7,500 transverse component body wave and 8,000 surface wave seismograms and the *NACT* and *IW* approaches, we discuss the relative performance of the path average approximation (*PAVA*), a zeroth order theoretical approximation appropriate for single mode surface waves, relative to *NACT* and compare the *IW* windowing scheme with a more standard 'full window' (*FW*) approach, in which a single time window is considered from the first body wave arrival to the fundamental mode surface waves. The combination *PAVA*/*FW* is often used in global tomography to supplement the travel time data.

We show that although the quality of the image derived under *PAVA*/*FW* formalism is very similar to that derived under *NACT*/*IW* in the first 300 km of the upper-mantle, where the resolution is dominated by surface waves, it deteriorates at greater depths. Images of the lower mantle are shown to be strongly sensitive to the theoretical formalism. In contrast, resolution of structure near the core-mantle boundary depends mostly on the windowing scheme. This is because this resolution is controlled by low amplitude phases such as S_{diff}, which are downweighted in the *FW* scheme. While the image obtained in D" using the combination *NACT/IW* is in good agreement with images obtained by other authors using both waveforms and travel times, we show that, when using *FW*, uppermost mantle structure can be mapped into D". This result is confirmed by synthetic tests performed on a composite of the upper mantle geodynamic model 3SMAC. We also show, based on synthetic tests, that, for structures in the upper mantle with sharp boundaries, differences are observed between *NACT* and *PAVA*. While a combination of travel times and surface wave data is adequate for resolving relatively smooth features in the mantle, our results show that, by potentially increasing the achievable sampling, the waveform approach shows great promise for future high-resolution tomographic modeling of mantle structure, if cast in appropriate theoretical framework.

Keywords: Tomography, mode coupling, synthetic waveforms, global seismology, Earth's interior, mantle

Introduction

Waveform tomography bears promises for the resolution of detailed structure in Earth's mantle in that it provides the means to utilize all of the information in the seismogram, rather than being limited to isolated phases as is the case in traveltime tomography. Synthetic seismogram computations are generally performed in a normal mode framework. The theoretical formalism involved in the exact modeling of a waveform through an arbitrarily heterogeneous medium is complex and the computation time prohibitive in the context of most computational environments [e.g. *Lognonné and Romanowicz*, 1990, *Geller and Takeuchi*, 1995]. Various simplifications thus need to be made to render the problem tractable. In the last fifteen years, several seismic waveform modeling techniques have been developed with the purpose of computing three-dimensional models of seismic wave velocity in the Earth in a reasonable time frame. The nature of the approximation used as well as the way in which the individual phases are weighted can significantly impact the ability to image heterogeneity.
Most global waveform tomographic studies rely on a zeroth order asymptotic expansion, the 'Path Average Approximation' (*PAVA*) [*Jordan*, 1978 ; *Woodhouse & Dziewonski*, 1984]. Under *PAVA*, sensitivity of the waveform is restricted to the horizontally averaged structure between the source and the receiver in the vertical plane containing the great-circle path. The path average phase perturbation is expressed as the average along the raypath of the local frequencies $\delta\omega^k_{local}$ as defined by Jordan (1978). To zeroth order in ℓ (where ℓ is the angular degree of the mode), *PAVA* is equivalent to taking into account the coupling of multiplets along a dispersion branch [*Mochizuki*, 1986, *Park*, 1987, *Romanowicz*, 1987], an approximation which is reasonably accurate for surface waves. Because it offers the important advantage of being relatively fast computationally, *PAVA* has also been applied to model body waves, although it is not able to reproduce the "ray" character of the path. In tomographic applications, it has been used to compute several mantle models [e.g. *Woodhouse & Dziewonski*, 1984,

Tanimoto, 1990] and has been augmented with traveltime data in more recent models, under the infinite frequency, ray theory approximation [e.g. *Su et al.*, 1994, *Liu & Dziewonski*, 1994] in order to improve resolution in the lower mantle.

To correctly account for the sensitivity of broadband body waves to the three-dimensional structure along the raypath it is necessary to include the effect of coupling across mode branches in the mode summation [e.g. *Romanowicz*, 1987, *Li & Tanimoto*, 1993]. In the Nonlinear Asymptotic Coupling Theory formalism (*NACT*) [*Li & Romanowicz*, 1995], only the term corresponding to across-branch coupling is linearized under the assumption of smoothness of heterogeneity. The path average contribution to the seismogram remains nonlinear, which improves the validity of the approach beyond the strictly short-time approximation of Li & Tanimoto (1993). To order zero in the asymptotic formalism, off-plane effects, i.e. focusing and defocusing of energy affecting wave amplitudes [*Romanowicz*, 1987], are not accounted for. Inclusion of such effects has been discussed for example by Clévédé & Lognonné (1996) and Marquering et al. (1998).

The whole-mantle shear velocity model SAW12D [*Li & Romanowicz*, 1996] has been developed in the *NACT* framework. Comparisons of 'checkerboard' tests have shown increased resolution in lower mantle over models derived under *PAVA* formalism [*Li & Romanowicz*, 1995]. SAW12D also presents good agreement with the results of local modeling of heterogeneity in the lowermost mantle [*Bréger et al.*, 1997].

In addition to an improved theoretical formalism, SAW12D was developed using a windowing scheme which we call the 'individual wavepacket' technique (*IW*) designed to allow relative weighting of individual energy wavepackets. The *IW* windowing consists in extracting separately the individual body wave energy packets in each seismic trace (figure 1, bottom). A data weighting scheme that normalizes the individual wavepacket amplitudes brings out the signal from the low-amplitude arrivals, and simultaneously allows each waveform to be fit independently. This method contrasts with the traditional

approach where a single wavepacket consisting of a continuous train of phases starting with the first energy arrival above the noise level (figure 1, top) is extracted. We refer here to this windowing scheme as the 'full waveform' (*FW*) technique. This procedure is widespread [e.g. *Tanimoto*, 1990, *Su et al.*, 1994] and has the advantage of allowing the rapid aquisition of a large quantity of data. However, the resulting models are influenced mostly by the information contained in the high amplitude phases, at the detriment of low-energy wavepackets such as, for example, the S_{diff} diffracted along the core-mantle boundary. This is because, in minimizing the difference between the data and the corresponding synthetics, the inversion will preferentially satisfy the constraints imposed by the high amplitude part of the wavepacket.
The *IW* method requires considerably more processing effort than the *FW* approach but it is crucial for the extraction of information related to the structure located in the lowermost part of the mantle, as the low amplitude S_{diff} phase is arguably the most valuable source of information relative to D" heterogeneity in a transverse component seismogram. Since low amplitude signal is enhanced in this method, it has the potential of increasing the effect of noise. However, our data selection is entirely manual. For each deconvolved and filtered seismogram, we compute the corresponding synthetic in the reference PREM model and compare it to the observed one, both visually and using a variance reduction criterion for each wavepacket considered. In this fashion, noisy data are readily rejected as well as records affected by timing errors and errors in instrument corrections.

The issue we wish to address here is what are the relative benefits of the theoretical improvements of *NACT* over *PAVA* and the windowing of individual energy wavepackets versus considering the body wave part of the seismogram as a whole. To quantify these benefits, we compare four tomographic models resulting from the inversion of a dataset under *PAVA* and *NACT* formalisms making use of the *FW* and IW windowing schemes. Ideally, one would want to use as reference a model obtained with a more exact theoretical formalism (ie: *Lognonné & Romanowicz*, 1990, *Geller & Takeuchi*, 1995, *Friederich*, 1998). However, computations for a degree 12 whole mantle model, the number of paths considered in our study and the necessary bandwidth (down to periods of 32 seconds) are currently beyond reach. We therefore use as reference the *NACT-IW* model, as it is the one derived with the most 'exact' theoretical formalism and the most sophisticated procedure that we can currently afford. We then observe and quantify how the image changes as a result of the use of a different windowing scheme (*FW*), a less accurate theoretical formalism (*PAVA*), and both. While we cannot prove rigorously that the *NACT-IW* approach is the 'best' possible one, differences in the models can help gain insight into the relative importance of various inversion ingredients in different depth ranges in the mantle. In addition, resolution tests for up to degree 8 (*Li & Romanowicz*, 1995, figures 5 & 6) and 12 (*Li & Romanowicz*, 1995, figure 6) constitute further evidence that *NACT* resolves the lower mantle better than *PAVA*.

Inversion

We use the same inversion procedure as that used by Li & Romanowicz (1996). A detailed description is given in that paper and we present here a synopsis of its most relevant aspects.

The inverse problem is solved by making use of a stochastic formulation [e.g. *Jackson*, 1979 ; *Tarantola & Valette*, 1982] and the finite-dimensional model is obtained by the recursive application of a Newton scheme to the Fréchet derivatives of the L^2-norm objective function. The *a priori* conditions imposed through the model covariance matrix have been kept identical in the derivation of each of the four solutions. The models are expressed as relative perturbations in shear wave velocity $\delta ln(V_{SH})$ from the spherically symmetric model PREM [*Dziewonski & Anderson*, 1981] and are parametrized laterally in spherical harmonics up to degree 12 and radially in Legendre polynomials up to degree 5 in the upper mantle and up to degree 7 in the lower mantle. The data are weighted by three factors ω_e, ω_n and ω_r. Each wavepacket is scaled by $\omega \equiv \omega_e \omega_n \omega_r$. The weight ω_e corresponds to systematic error (uncertainty in source parameters, off-great circle effects, small scale heterogeneity, etc...) which is scaled to the amplitude of the wavepacket such that $\omega_e = \frac{1}{\epsilon}$ where ϵ is the rms of the wavepacket. The weight ω_n accounts for the redundancy in the data that constitutes a given wavepacket and is computed as the geometric average of the two extremes: for no redundancy in the wavepacket, ω_n should be set to unity. In contrast, for totally redundant data, ω_n should be $\frac{1}{n}$ where n is the number of data points in the wavepacket. We thus set $\omega_n \equiv n^{-\frac{1}{2}}$. Finally, a factor ω_r accounts for the redundancy among wavepackets. A full description of its computation is given in Li & Romanowicz (1996), Appendix A. Hereafter, we use the nomenclature given in Table 1 to refer to the four combinations of models derived. Horizontal comparisons (ie: between models 1 and 2 or 3 and 4) provide information on the incidence of the theoretical formalism on the models. In contrast, vertical comparisons (ie: between models 1 and 3 or 2 and 4) bring out the impact of the windowing scheme.

Dataset

We use a set of transverse component accelerograms, consisting of 7,527 body wave traces low-pass filtered at 32 seconds and 7,919 first and second orbit Love wavetrains low-passed at 80 seconds collected from GSN, GDSN and GEOSCOPE networks between 1977 and 1992. The same dataset has been used in the computation of each of models 1 through 4.

Results

In figure 2, we present the correlation as a function of depth of model 1 with the models resulting from each of the other three inversions. The solid line (labeled 2) represents the correlation between the *NACT* and the *PAVA* formalism. In contrast, the dashed line (labeled 3) shows the correlation between *IW* and *FW*-derived models under *NACT* formalism. The dotted line (labeled 4) shows the decorrelation due to the combined use of the *PAVA* formalism with the *FW* scheme.

1. Uppermost mantle

In the first 300 km of the mantle, models 2 and 3 remain very similar to NACT-IW (Figure 2). The comparison between the heterogeneity pattern at 150 km (Figure 3 (top) and Table 2 a)) shows nearly perfect correlation among models at that depth: in all cases, the major global tectonic features are well recovered. The first 300 km of the mantle are predominantly sampled by the Love wavetrains for which the *PAVA* approximation works well, as discussed above. Since the difference between *IW* and *FW* schemes applies predominantly to the modeling of body waveforms, the windowing scheme shows little impact on the tomographic image of the uppermost mantle. The similarity among these four images also indicates that the sets of damping parameters used in each inversion have been properly calibrated. Except for smoothness across the 670 km discontinuity, the differences among the models at depths other than the uppermost mantle are unlikely to be caused by inconsistencies in the a priori conditions imposed to regulate the inversion. We address the issue of the smoothness constraint between upper and lower mantle below.

2. Transition zone

The similarity between models decreases continuously below a depth of 300 km. In the lower part of the upper mantle, models 2 and 3 remain correlated with model 1 at the 0.90 level but the effect of the adoption of *PAVA* combined with *FW* brings the correlation between models 1 and 4 below 0.80 at the bottom of the transition zone (Figure 2). The near overlap between the correlation profiles of models 2 and 3 indicates that theoretical formalism and windowing scheme in the upper mantle contribute equally to the quality of the tomographic image. In Figure 3 (bottom) and Table 2 b), we compare the models at 600 km depth. Important features such as the westward shift with depth of low velocities in the Central Pacific [e.g. *Romanowicz et al.*, 1987] is present in all four models. However, the model details are somewhat displaced in the *PAVA* images, in particular under the Southern Pacific and the South-American craton and the amplitudes are decreased in the *FW*-derived models. The issue of model amplitude is closely related to damping in the inversion. Our experience is that slight adjustment of damping to obtain a closer match of the amplitudes in different models is always possible. However, it will not affect the geographical distribution of model heterogeneity.

3. Lower mantle

In the lower mantle, the progressive decorrelation between models 1 and 2 (Figure 2) illustrates the importance of the choice of an accurate theoretical formalism in a region sampled predominantly by large amplitude body wave phases such as S and its multiples, down to 2,500 km depth. Figure 4 (top) shows maps of heterogeneity at a depth of 1,500 km where models 1 and 2 are least similar. Differences in amplitudes are observed under the Asian continent and the models differ most in pattern under the Arctic, the Central and North Eastern Pacific, the South Western Atlantic and the North and South American cratons. The same discrepancies persist in the comparison between the *FW* models 3 and 4, providing further evidence that the effect of the theory dominates the resolution of structure in the lower mantle. Comparison between the end member models 1 and 4 shows disagreement in most regions of the globe, with correlation falling to 0.50 at 2,300 km. In most of the lower mantle the choice of windowing has a minor importance, (see the similarity in correlation level between models 2 and 4 between 1,000 km and 2,500 km depth). The decorrelation from *IW-NACT* to *FW-NACT* (or *IW-PAVA* to *FW-PAVA*) is indeed small compared to that resulting from the passage from *IW-NACT* to *IW-PAVA* (see table 2 c)).

4. D" region

In the lowermost mantle, the resolution is driven by the fit to the ScS phase and its multiples reflected on the core-mantle boundary, and the low amplitude S_{diff} phase. In figure 5, we present a projection on the CMB of the coverage by 954 S_{diff}, 3,766 ScS, 1,539 ScS_2 and 125 ScS_3 phases. The linear features represent the sampling by S_{diff} and the circles correspond to the CMB reflections of ScS and its multiples. This projection is calculated in the ray theoretic approximation (no Fresnel zone is computed) and thus represents a lower bound of our D" coverage. Due to inhomogeneous sampling, the northern hemisphere is expected to be better resolved than the southern hemisphere. As discussed above, resolution at these depths is expected to be highly sensitive to the windowing scheme because of the relatively low amplitude of S_{diff}. Figure 4 (bottom) shows considerable differences between models obtained using the two different windowing schemes, with the correlation coefficient falling below 0.70 (see table 2 d)). A noticeable distortion arising from the use of *FW* is the change in sign of the anomaly under the Southern African craton present both in *NACT* and *PAVA* models. More importantly, the D" structure in the models derived with *FW* is found to be correlated at up to the 0.85 level with that of the heterogeneity at 150 km depth in the *NACT-IW* model. Table 2 d) also shows that the *FW* models in the D" region are seen to correlate better with the heterogeneity at 150 km (correlation coefficient of 0.80) than with their *IW* counterparts in the D" (correlation coefficient of 0.70). This effect is absent in the models derived with the *IW* scheme where little correlation is observed between the uppermost mantle and the D" (correlation coefficient of 0.33). In figure 6, we present the spherical harmonic degree-by-degree correlation between uppermost mantle and D" heterogeneity for all models. Models derived with the *IW* scheme in the *NACT* (solid line-diamonds) and *PAVA* (dashed line-circles) formalisms are poorly correlated with the surface at all degrees (correlation coefficient between 0 and 0.60), except at degree 1. Conversely, the models derived with the *FW* scheme (dotted line-squares for *NACT* and long dashed line-triangle for *PAVA*) correlate strongly except at degrees 2 and 3 and culminate at degrees 4 to 6 which correspond to the spectral signature of tectonics.

Our results show that upper mantle structure is being mapped into the lower mantle at degrees higher than 3 when the *FW* formalism is used. This effect can be understood in the following way: lateral heterogeneity is strongest in the uppermost 200 km of the mantle, and the least squares inversion procedure (L^2 norm constraint in the inversion) will have a tendency to map the unexplained part of the signal into the least sampled regions of the model. This is possible because, although the parametrization is split across the 670 km discontinuity, imposition of a smoothness constraint between upper and lower mantle is necessary to maintain continuity in the model rms. We indeed observe wide fluctuations in transition zone and uppermost lower mantle amplitudes in the absence of smoothness constraints at the discontinuity. A similar trade-off would of course also be observed for a 'whole mantle' radial parametrization, using either local or global basis functions, in the presence of radial damping.

It thus appears that, in the absence of S_{diff} coverage, the lowermost mantle is poorly sampled and acts as repository for model nullspace. To verify that this is indeed the case, we conduct an *IW-PAVA* inversion where we exclude from the data set the wavepackets corresponding to S_{diff} and ScS phase arrivals. Figure 7 shows the result of this experiment. The top left figure shows model 2 at 2,800 km depth where all the data have been included and the correlation with the structure at 150 km is weak (correlation coefficient of 0.36). The top right figure shows the D" structure after inversion of the data set without the S_{diff} phases. The correlation with the uppermost mantle increases to 0.57. In the bottom left figure, the S_{diff} and the ScS phases have been taken out of the data set and the correlation reaches with upper mantle 0.88. We show in the bottom right part of the figure model 2 at 150 km depth for comparison. This test demonstrates that the absence of sampling in the lowermost mantle produces the transfer of heterogeneity from the uppermost mantle in the inversion. This effect is seen to become more prominent as the sampling of D" diminishes. This is precisely what is observed in the *PAVA-FW* inversion of the full dataset, an indication that, because it fails to take the S_{diff} into account, this methodology misses to a large extent information relative to the lowermost mantle. This is one of the reasons why studies that rely on *PAVA-FW* formalism augment their dataset with traveltime data of phases sensitive to the lowermost mantle.

Synthetic tests

Mapping of upper mantle heterogeneity in the D"

The analysis performed so far has relied on the postulate that of all the formalisms presented so far, the *NACT-IW* best images the structure sampled. Although plausible, this remains an assumption. A more unbiased approach to measuring the distortion resulting from the use of either formalism is to perform a synthetic test on a model with realistic upper mantle and no lower mantle 3D structure. Ideally, this test would be performed by tracing 'exact' synthetics (ie: non-asymptotic) through the input model and by inverting them using each of the four methods. As indicated above, there nevertheless doesn't exist any method that allows the computation of a synthetic data set of the size used in the present study in a reasonnable amount of time. An element of currently unavoidable circularity is therefore present in the models derived from synthetic tests preformed with *NACT*. It is nevertheless instructive to examine the differences between models obtained using various approaches.

We compute synthetic seismograms for the paths used in the inversions described above using as input the geodynamic model 3SMAC [*Nataf & Ricard*, 1996] between 50 km and 600 km depths and spherically symmetric model PREM [*Dziewonski & Anderson*, 1981] in the rest of the mantle. The input model model is parametrized radially in Legendre polynomials up to degree 5 in the upper mantle. *NACT* synthetics are traced through the composite model expanded laterally up to spherical harmonic degree 32 (Figure 8) and inverted in *NACT-IW* and *PAVA-FW* formalisms for up to degree 12, thus allowing for aliasing of small-scale heterogeneity into the long-wavelength model [e.g. *Mégnin et al.*, 1997]. In the upper mantle, we compare the input model truncated to degree 12 (Figure 8) to the result of the *NACT-IW* (Figure 9) and the *PAVA-FW* (Figure 10) inversions. In the lower mantle (Figures 9 and 10), the heterogeneity recovered is spurious.

At 100 and 200 km depths (Figures 9 and 10), the heterogeneity pattern of the input model is largely recovered by both inversion schemes, although the amplitudes are slightly depressed, in general agreement with a similar test made with phase velocities by Ricard et al. (1996). In agreement with the observations from the inversion of the 'real' dataset, the models exhibit little dependence on the formalism, owing to the dominance of surface waves well described under *PAVA* theory.

Radial smearing of the heterogeneity is observed between 300 and 400 km depths. This region corresponds to a sharp drop in coverage owing to the diminishing Love wave sampling which causes a downward transfer of heterogeneity. This effect is compensated at 500 km (and 600 km with *PAVA-FW*) by the appearance of 'negative tectonic features', in particular over the Asian, North American and South American shields. We note nevertheless that the amplitude of this effect is modest (not exceeding $\pm 1\%$) compared with amplitudes recovered from real datasets and may be further diminished by the adoption of local basis functions such as splines (e.g. *Masters et al.*, 1996, *Su & Dziewonski*, 1996) to parametrize the model.

In the lower mantle, (Figures 9 and 10) the *PAVA-FW* models show more heterogeneity than the *NACT-IW* at nearly all depths. In particular at 2,800 km, heterogeneity resulting from the projection of the uppermost mantle structure is observed with amplitude peaks nearing 2%, an effect largely absent in the *NACT-IW* inversion. The *PAVA-FW* image is indeed characterized by amplitudes larger than 1%, coinciding with the surface location of the African Craton and the North and South American shields. Negative peaks exceeding -1% are also observed below the East Pacific Rise, the SouthEast Indian Ridge and the southernmost part of the Mid-Atlantic Ridge. In contrast, the *NACT-IW* amplitudes are almost everywhere less than the smallest contour gradation (1%) and nowhere related to uppermost mantle structure. This is in agreement with the conclusions from the inversion of real data and thus confirms the predominance of this effect with *PAVA-FW* tomography.

Surface wave tomography: *NACT* **vs** *PAVA*

The results in the upper mantle show that, although compatible, *PAVA* and *NACT* models differ somewhat in the depth range sampled mostly by Love waves. Discrepancies between the two formalisms result from the absence of coupling across mode branches in *PAVA* that may affect wavepackets that include higher mode energy in addition to the fundamental mode. To assess the impact of these differences on upper mantle structure, we trace 7,919 *NACT* Love wave synthetics through a model consisting of a fast and a slow heterogeneity of identical dimensions buried between 200 and 600 km depth and latitudes 0° and 45°. The fast heterogeneity covers longitudes from 135° to 180° and the slow heterogeneity from 180° to 225° (Figure 11). The model is expanded laterally up to spherical harmonic degree 12 and radially in legendre polynomials up to degree 5. We then invert the synthetic dataset using *NACT* and *PAVA* formalisms for heterogeneity up to degree 12. For computational reasons, the low-pass cutoff frequency has been decreased from 12.5 mHz to 8 mHz (80 to 125 seconds). In Figure 11 (center) , we show the result of the *NACT* inversion. Although some radial smearing is observed, (compare with the input model at 650 km), the lateral pattern is almost perfectly recovered: even the Gibbs oscillations resulting from the truncation in the spherical harmonics expansion have been preserved in the *NACT* inversion. The *PAVA* inversion on the other hand results in significant loss of the input signal: the shape of the heterogeneity has been distorted and projected southward after an inversion of polarity (note the appearance of the mirror image of the heterogeneity pattern between 250 km and 400 km between latitudes 0° and 45° south).

A different view of that difference is seen in the spectral heterogeneity maps of figure 12 (top) where the amplitude of the heterogeneity for each model is plotted as a function of wavelength (horizontal axis) depth in the upper mantle (vertical axis). The left figure shows the input model (the spectral equivalent of Figure 11) which displays a strong signal between degrees 1 and 7 and above degree 10, with an amplitude peak at degree

4. In the middle figure, the model resulting from the *NACT* inversion is presented (equivalent to Figure 11, center), displaying some radial smearing of the low degrees but an overall good restitution of the input image. To the right, the *PAVA* inversion is plotted (equivalent to Figure 11, right), showing leakage across heterogeneity of different wavelengths (note for example that the strong degree 9 signal between 200 and 400 km depth is entirely absent from the input model). At the far right of the figure, the rms amplitude of the input model (solid line), the *NACT* (dashed line) and the *PAVA* inversions (dotted line) is plotted as a function of depth. The radial agreement between input and *NACT* models is quite good. On the other hand, the overshoot of the *PAVA* model in the uppermost mantle is compensated at depth, in particular at 300 km and 500 km.

We finally investigate the transfer of heterogeneity across wavelengths, observed above when using the *PAVA* formalism, by tracing the same set of *NACT* Love wave synthetics through the synthetic model, expanded this time up to spherical harmonic degree 6, and inverting it for up to degree 12 in *NACT* and *PAVA* formalisms. The result is shown in figure 12 (bottom). At the left, the input model is plotted. The middle figure shows the result of the *NACT* inversion. No leakage of heterogeneity is detected across wavelengths. At the right the *PAVA* inversion show significant transfer of heterogeneity from the long into the short wavelengths, representing on average 25% of the input structure and peaking at 50% (e.g. at degree 11 between 200 km and 300 km depth). This is a direct consequence of the difference between the two theoretical formalisms in the context of surface waves: the *PAVA* inversion compensates the inability to fit the *NACT* synthetics by introducing ghost structure at high degrees.

Discussion and conclusions

We have shown that two improvements to the common path average-'full window' data selection inversion procedure have a significant effect on the tomographic image: a more accurate theoretical formalism such as the nonlinear asymptotic coupling theory (*NACT*) which allows the modeling- of the two-dimensional sensitivity along the great circle ray path, and a windowing scheme that extracts separately the energy wavepackets in a seismic trace. However, these improvements have different effects on the resolution of the tomographic image at different mantle depths. The uppermost regions of the mantle, sampled predominantly by surface waves, are not affected much by the choice of theoretical formalism or the windowing scheme applied to the body waveforms. Images of the mid-mantle, sampled by large amplitude body waves, are strongly dependent on the choice of theoretical formalism, as illustrated by the differences resulting from the passage from *NACT* to *PAVA* formalism. In contrast, in the lowermost mantle, sampled to a large extent by low energy phases, the choice of a windowing scheme that enhances the contribution of these phases is critical in order to avoid mapping of upper mantle structure into this part of the earth. In the models shown, the combination of *PAVA* with *FW* (and, to a similar extent, of *NACT* with *FW*) projects tectonic features into the D" region. This effect is not present when the *NACT* formalism is used in conjunction with an 'individual wavepacket' windowing scheme. This result is independently confirmed by the application of a synthetic test using the geodynamic model *3SMAC*.

By conducting another synthetic test with Love waves on a simple heterogeneity pattern in the upper mantle, we oberved noticeable differences between *NACT* and PAVA-derived models. This is likely due to the coupling between the fundamental and the harmonic branches in *NACT*, for surface wavepackets with group velocity windows which contain higher mode energy.

We note that other global mantle tomographic models that have been derived using, in particular, body waveforms under the *PAVA* approximation [e.g. *Su et al.*, 1994] fortunately do not show the pervasive mapping of uppermost mantle structure into D". This is because these studies combine the waveform dataset with a large dataset of travel times of isolated bodywave phases, such as multiple S and ScS, which provide them with resolution in the lower mantle. This is arguably a valid approach when the focus is long wavelength structure such as currently recovered [*Su et al.*, 1994, *Masters et al.*, 1996, *Liu & Dziewonski*, 1997]. Nevertheless, the poor performance of the *PAVA-FW* approach in the recovery of lowermost mantle heterogeneity casts a doubt on the appropriateness of supplementing the travel time data set with body waveforms fit under a formalism designed for surface wave tomography. As more and more attention is given to smaller scale detail, the accuracy of the theoretical formalism will become critical in recovering unbiased distribution of lateral heterogeneity in the deep mantle. We have shown in this paper that, with appropriate methodology, a data set of well-distributed waveforms alone can be used to recover structure in the deep mantle. The use of travel-times in combination with waveforms has several limitations. The necessity of using isolated seismic phases limits the sampling of the mantle that can be achieved. Moreover, travel times, as currently used, are inverted using kernels appropriate for infinite frequency ray theory, which assumes that the sensitivity to structure is 1) limited to the infinitely narrow raypath, 2) distributed uniformely along the raypath. For broadband bodywaves, these assumptions are inaccurate [e.g. *Stark & Nikolayev*, 1993, *Tanimoto*, 1995] and may lead to further biases in the recovered lower mantle structure. We are presently investigating this issue.

The set of experiments presented in this paper is limited in that the reference framework for forward and inverse modeling is that of the approximate *NACT* theory, rather than an exact computation of seismograms in the 3D earth. Computing exact bodywave seismograms for a realistic path coverage in a degree 12 earth model down to periods of 30 seconds still represents a formidable computational task. In a related study, we are nevertheless addressing the performance of *NACT* and *PAVA* versus more exact computations in the upper mantle, using surface wave data down to periods of 80 sec [*Clévédé et al.*, in preparation].

Although the combination of *NACT* with *IW* does much to enhance the resolution in the lower mantle, seismic tomography can still greatly benefit from a variety of improvements in the waveform inversion techniques. The modeling of sensitivity to off-great circle plane heterogeneity can bring another level of improvement to the modelisation of waveforms as it allows to take into account elastic effects on wave amplitudes. This can be achieved by using higher order asymptotics [e.g. *Romanowicz*, 1987, *Marquering et al.*, 1998] and, eventually, accurate higher order perturbation theory [e.g. *Lognonné & Clévédé*, 1997].

Acknowledgments

We thank Wolfgang Friederich and an anonymous reviewer for insightful suggestions and Éric Clévédé for fruitful discussions. Berkeley Seismological Laboratory contribution 99-01.

References

Bréger, L., Romanowicz, B. and Vinnik, L., 1997. Test of tomographic models of D" using differential travel time data, *Geophys. Res. Lett.*, **25**, 5-8.

Clévédé, É., Mégnin, C., Romanowicz,B. and Lognonné, P., 1998. Seismic waveform modeling in a three-dimensional Earth: asymptotic and non-asymptotic approaches, submitted to *Phys. Earth planet. Inter.*.

Clévédé, É. and Lognonné, P. 1996. Fréchet derivatives of coupled seismograms with respect to an anelastic rotating Earth, *Geophys. J. Int.*, **124**, 456-482.

Dziewonski, A.M. and Anderson, D.L., 1981. Preliminary reference Earth model, *Phys. Earth planet. Inter.,* **25**, 297-356.

Friederich, W. 1998. Wave-theoretical inversion of teleseismic surface waves in a regional network; phase-velocity maps and a three-dimensional upper-mantle shear-wave-velocity model for southern Germany, *Geophys. J. Int.* **132**, 203-225.

Geller, R.J. and Takeuchi, N., 1995. A new method for computing highly accurate DSM synthetic seismograms, *Geophys. J. Int.*, **123**, 449-470.

Jordan, T.H., 1978. A procedure for estimating lateral variations from low-frequency eigenspectra data, *Geophys. J. R. Astr. Soc.*, **52**, 441-455.

Jackson, D. D., 1979. The use of a priori data to resolve non-uniqueness in linear inversion, *Geophys. J. R. Astr. Soc.*, **57**, 137-157.

Li, X.D. and Romanowicz, B., 1996. Global mantle shear-velocity model developed using nonlinear asymptotic coupling theory, *J. Geophys. Res.*, **101**, 22,245-22,272.

Li, X.D. and Romanowicz, B., 1995. Comparison of global waveform inversions with and without considering cross-branch modal coupling, *Geophys. J. Int.*, **121**, 695-709.

Li, X.D. and Tanimoto, T., 1993. Waveforms of long-period body waves in a slightly aspherical Earth model, *Geophys. J. R. Astr. Soc.*, **112**, 92-102.

Liu, X.-F. and Dziewonski, A.M., 1997. On the scale of heterogeneity in the lowermost mantle, *EOS Trans. AGU*, **78**, F17.

Liu, X.-F. and Dziewonski, A.M., 1994. Lowermost mantle shear wave velocity structure, *EOS Trans. AGU*, **75**, 663.

Lognonné, P., and Clévédé, É., 1997. Diffraction of long period Rayleigh waves by a slab: effects of mode coupling, *Geophys. Res. Lett.*, **24**, 1035-1038.

Lognonné, P., and Romanowicz, B., 1990. Modelling of coupled normal modes of the Earth: the spectral method, *Geophys. J. Int.*, **102**, 365-395.

Marquering, H., Nolet, G., and Dahlen, F.A., 1998. Three-dimensional waveform sensitivity kernels, *Geophys. J. Int.*, **132**, 521-534.

Masters, G., Johnson, S., Laske, G., and Bolton, H., 1996. A shear-velocity model of the mantle, *Phil. Trans. R. Soc. London*, **354** 1385-1410.

Mégnin, C., Bunge, H.P., Romanowicz, B. and Richards, M.A., 1997. Imaging 3-D spherical convection models : What can seismic tomography tell us about mantle dynamics?, *Geophys. Res. Lett.*, **24**, 1299-1303,

Mochizuki, E., 1986. Free oscillations and surface waves of an aspherical Earth, *Geophys. Res. Lett.*, **13**, 1478-1481.

Nataf, H.-C. and Ricard, Y., 1996. 3SMAC: an a priori tomographic model of the upper mantle based on geophysical modeling, *Phys. Earth planet. Inter.,* **95** 101-122.

Park, J., 1987. Asymptotic coupled mode expressions for multiplet amplitude anomalies and frequency shifts on an aspherical Earth, *Geophys. J. R. Astr. Soc.*, **90**, 129-169.

Ricard, Y., H.-C. Nataf and J.-P. Montagner, The three-dimensional seismological a priori model constrained: Confrontation with seismic data, *J. Geophys. Res.,* **101**, 8457-8472, 1996.

Romanowicz, B., 1987. Multiplet-multiplet coupling due to lateral heterogeneity: asymptotic effects on the amplitude and frequency of Earth's normal modes, *Geophys. J. R. Astr. Soc.*, **90**, 75-100.

Romanowicz, B., Roult G. and Kohl, T., 1987. The upper mantle degree two pattern: constraints from GEOSCOPE fundamental spheroidal mode eigenfrequency and attenuation measurements, *Geophys. Res. Lett.*, **14**, No. 12, 1219-1222.

Stark, P.B. and Nikolaiev, D.I., 1993. Toward tubular tomography, *J. Geophys. Res.*, **98**, 8095-8106,

Su, W.J., Woodward, R.L., and Dziewonski, A.M., 1994. Degree 12 model of shear velocity in the mantle, *J. Geophys. Res.,* **99**, 6945-6980.

Su, W.J., and Dziewonski, A.M., 1996. Global tomographic inversion using b-splines, *Eos Trans. AGU*, **77**(46), Fall Meet. Suppl..

Tanimoto, T., 1995. Formalism for traveltime inversion with finite frequency effects, *Geophys. J. Int.* **121**, 103-110.

Tanimoto, T., 1990. Long wavelength S-wave velocity structure throughout the mantle *Geophys. J. Int.*, **100**, 327-336.

Tanimoto, T., 1984. A simple derivation of the formula to calculate synthetic long-period seismograms in a heterogeneous earth by normal mode summation, *Geophys. J. R. Astr. Soc.*, **77**, 275-278.

Tarantola, A. and Valette, B., 1982. Generalized non-linear inverse problems solved using the least-squares criterion, *Rev. Geophys.,* **20**, 219-232.

Wang, Z. and Dahlen, F.A., 1995. Spherical spline parametrization of three-dimensional Earth models, *Geophys. Res. Lett.*, **22**, No. 22, 3099-3102.

Wessel, P. & W.H.F. Smith, 1991. New version of the Generic Mapping Tool released, *EOS Trans. AGU*, **72**, 441, 445-446.

Woodhouse, J.H., 1983. The joint inversion of seismic waveforms for lateral variations in Earth structure and eartquake source parameters, *Proc. 'Enrico Fermi' Int. Sch. Phys. LXXXV*, (eds Kanamori, H. & E. Boschi), 366-397.

Woodhouse, J.H. & Dziewonski, A.M., 1984. Mapping the upper mantle : Three dimensional modeling of Earth's structure by inversion of seismic waveforms, *J.*

Geophys. Res., **89**, 5,953-5,986.

This manuscript was prepared with the AGU LaTeX macros v3.1.

Table 1. Nomenclature of the four models computed in this study.

Table 2. a) Correlation between models at 150 km depth. As seen in the corrsponding figure (3, top) the models do not depend on which theoretical formalism and data selection scheme is used. b) Correlation between models at 600 km depth. Theory and windowing equally to the image quality. This table corresponds to figure 3, bottom. c) Correlation between models at 1500 km depth. The decorrelation due to the use of *PAVA* exceeds that due to *FW*. This table corresponds to figure 4, top. d) Correlation between models at 2800 km depth. Although the windowing is the most important factor, the theoretical framework contributes significantly to the image quality. The models are also correlated with with the structure at 150 km depth. The *FW* models at the CMB correlate better with the surface heterogeneity than they do wit htheir *IW* counterparts at the CMB. This table corresponds to figure 4, bottom.

Figure 1. Top trace: Full waveform selection scheme (FW). The entire body wavetrain is selected. High amplitude phases are preferentially fit in the inversion. Bottom trace: Individual wavepacket selection scheme (IW). The different energy wavepackets are selected and fit separately. The bodywaveforms selected for the inversion are the energy arrivals between the dashed vertical lines. The assignment of phase names to the extracted window is not required by the theory but is used in the weighting scheme to penalize redundant paths.

Figure 2. Correlation of the NACT-IW model with PAVA-IW (solid line) NACT-FW (dashed line) and PAVA-FW (dotted line). The model numbers correspond to those of Table 1.

Figure 3. top: Heterogeneity at 150 km depth derived from each waveform inversion technique. The structure is sampled predominantly by surface waves and no significant difference is observed among the various models. bottom: Heterogeneity at 600 km depth derived from each waveform inversion technique.

Figure 4. top: Heterogeneity at 1,500 km depth derived from each waveform inversion technique. This region is predominantly sampled by large amplitude body waves (S, SS, ...). The quality of the image at that depth is strongly dependent on the accuracy of the waveform modeling and weakly on the type of windowing scheme. bottom: Heterogeneity at 2,800 km depth derived from each waveform inversion technique. The use of a non-selective windowing scheme (bottom graphs) causes the mapping of surface heterogeneity at the CMB.

Figure 5. Coverage at the core-mantle boundary. The linear features represent the regions sampled by the 950 S_{diff} phases. The circles correspond to the 7,200 CMB reflections of the ScS, ScS_2 and ScS_3 phases.

Figure 6. Degree-by-degree correlation between surface (150 km) and D" (2,800 km) heterogeneity at each spherical harmonic degree for NACT-IW (solid lines-diamonds), PAVA-IW (dashed lines-circles), NACT-FW (dotted lines-squares) and PAVA-FW (long dashed lines-triangles)

Figure 7. Top left: Model 2 (*PAVA-IW*) at 2,800 km (same as [Figure 4, bottom] top right). Top right: *PAVA-IW* inversion of the data set without the S_{diff} phases. Bottom left *PAVA-IW* inversion of the data set without the S_{diff} and the ScS phases. Bottom right: Model 2 (*PAVA-IW*) at 150 km (same as Figure [3, top] top right).

Figure 8. Left: Input model 3SMAC expanded laterally up to spherical harmonic degree 32 and radially in Legendre polynomials up to degree 5. In the lower mantle, the input model is the spherically symmetric model PREM. Right: 3SMAC truncated at spherical harmonic degree 12.

Figure 9. NACT-IW inversion for up to spherical harmonic degree 12 of synthetics computed for the (degree 32) model in Figure 8.

Figure 10. PAVA-FW inversion for up to spherical harmonic degree 12 of synthetics computed for the (degree 32) model in Figure 8.

Figure 11. Left: Synthetic model used in the surface wave experiment. The heterogeneities are distributed radially between 200 and 600 km depth and laterally between latitudes 0° and 45° and longitudes from 135° to 180° (fast heterogeneity) and from 180° to 225° (slow heterogeneity). The model is expanded laterally in spherical harmonics up to degree 12 and radially in legendre polynomials up to degree 5.Center: $NACT$ inversion of synthetics through the synthetic model. Right: $PAVA$ inversion of synthetics through the synthetic model.

Figure 12. Spectral representation of the synthetic experiments. Amplitudes are plotted for each model as function of spherical harmonic degree (horizontal axis) and depth (vertical axis). Top: left: input synthetic model (Figure 11, left). Center: $NACT$ inversion (Figure 11, center). Right: $PAVA$ inversion (Figure 11, right). Far right: rms amplitudes for -solid line- the input model, -dashed line- the $NACT$ model, and -dotted line- the $PAVA$ model. Bottom: left: input synthetic model (smax=6). Center: $NACT$ inversion for up to degree 12. Right: $PAVA$ inversion for up to degree 12. Far right: rms amplitudes for -solid line- the input model, -dashed line- the $NACT$ model, and -dotted line- the $PAVA$ model.

Data selection scheme / Theory	$NACT$	$PAVA$
Individual wavepacket (IW)	1	2
Full waveform (FW)	3	4

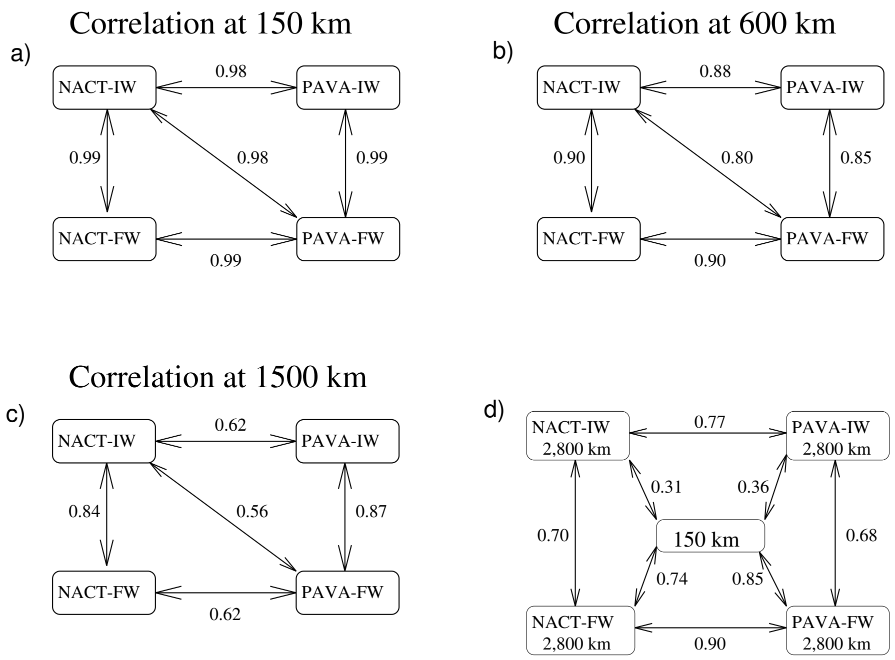
Correlation at 150 km
a)
NACT-IW
PAVA-IW
NACT-FW
PAVA-FW
0.98
0.99
0.98
0.99
0.99
Correlation at 600 km
b)
NACT-IW
PAVA-IW
NACT-FW
PAVA-FW
0.88
0.90
0.80
0.85
0.90
Correlation at 1500 km
c)
NACT-IW
PAVA-IW
NACT-FW
PAVA-FW
0.62
0.84
0.56
0.87
0.62
d)
NACT-IW 2,800 km
PAVA-IW 2,800 km
150 km
NACT-FW 2,800 km
PAVA-FW 2,800 km
0.77
0.31
0.36
0.70
0.68
0.74
0.85
0.90

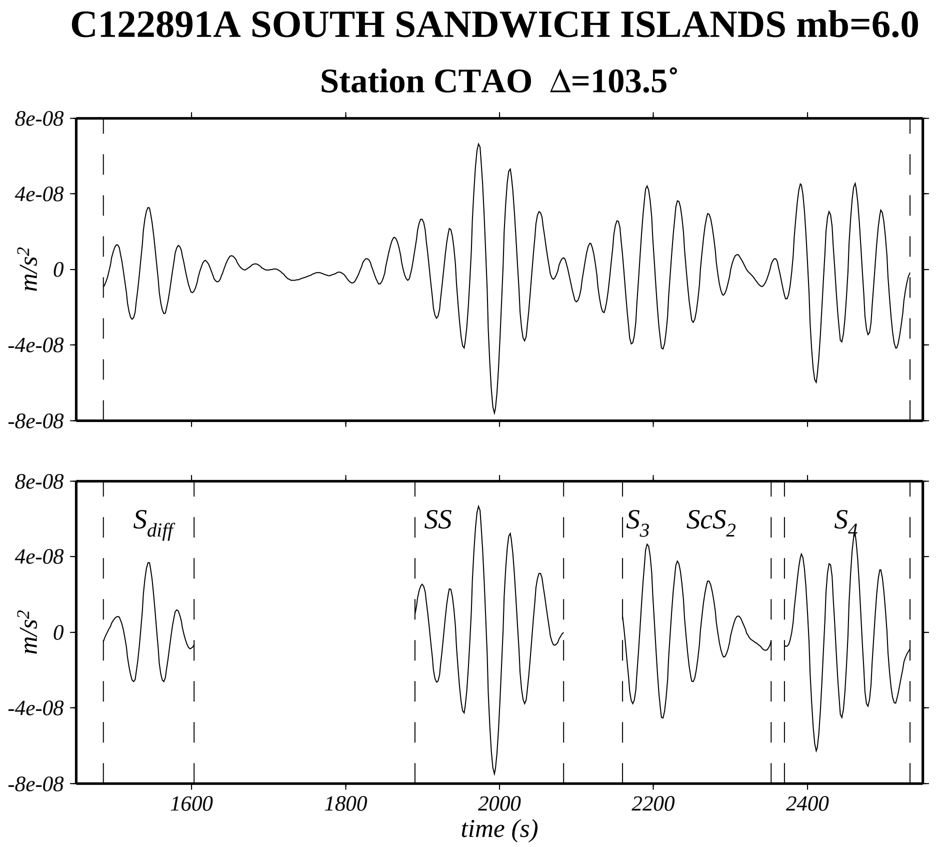
C122891A SOUTH SANDWICH ISLANDS mb=6.0
Station CTAO Δ=103.5˚
8e-08
4e-08
0
-4e-08
-8e-08
m/s²
S_{diff}
SS
S_3
ScS_2
S_4
1600
1800
2000
2200
2400
time (s)

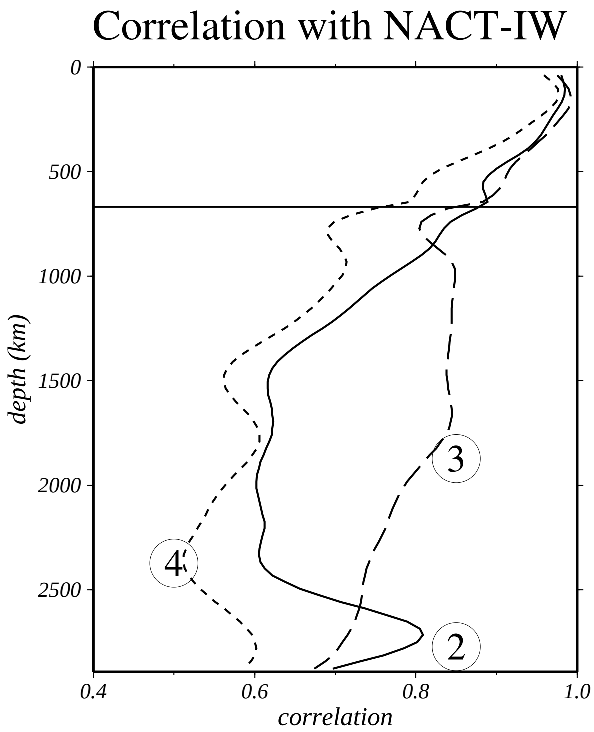

Correlation with NACT-IW
0
500
1000
1500
2000
2500
depth (km)
0.4
0.6
0.8
1.0
correlation
2
3
4

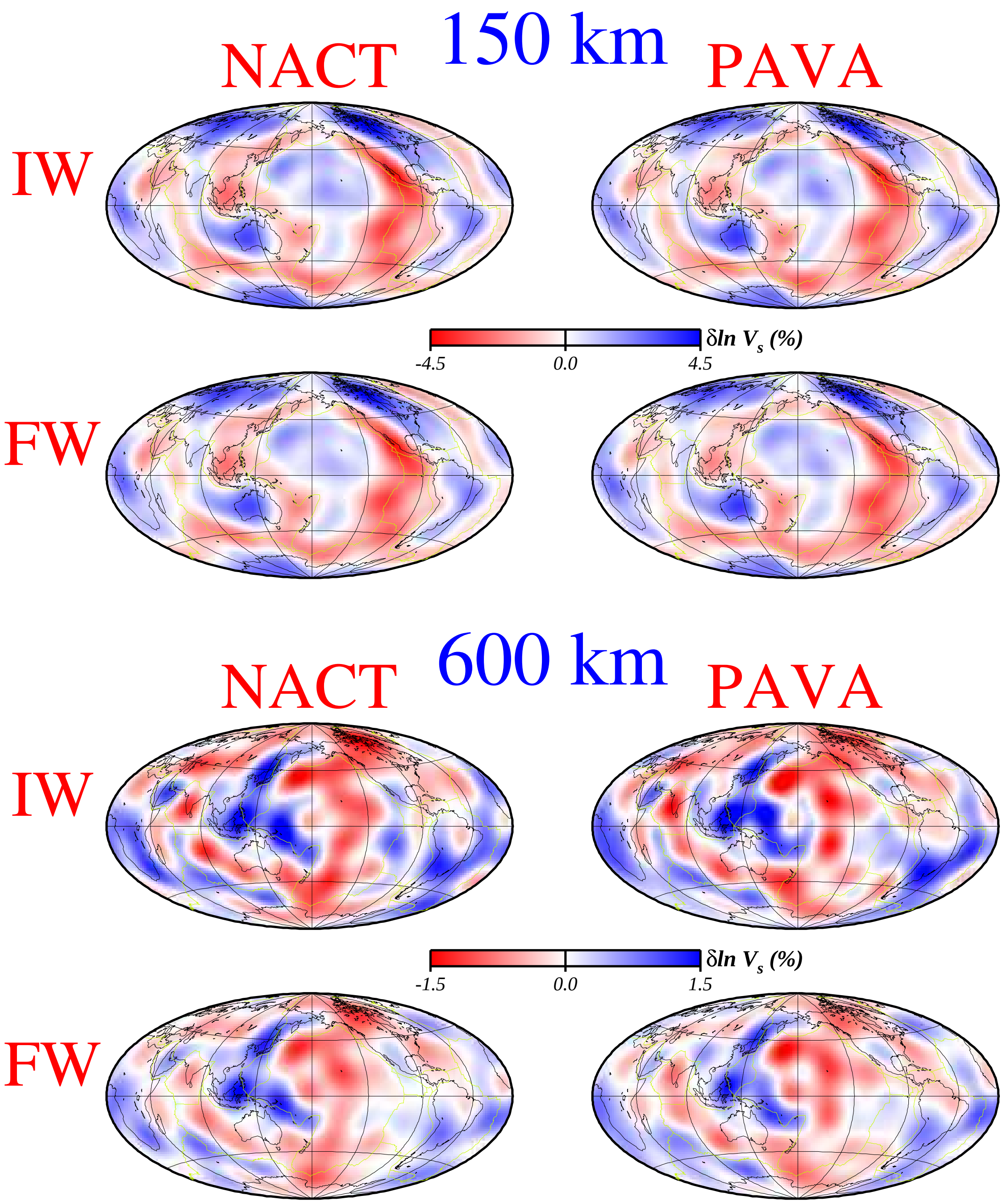
150 km
NACT
PAVA
IW
FW
δln V_s (%)
-4.5
0.0
4.5
600 km
NACT
PAVA
IW
FW
δln V_s (%)
-1.5
0.0
1.5

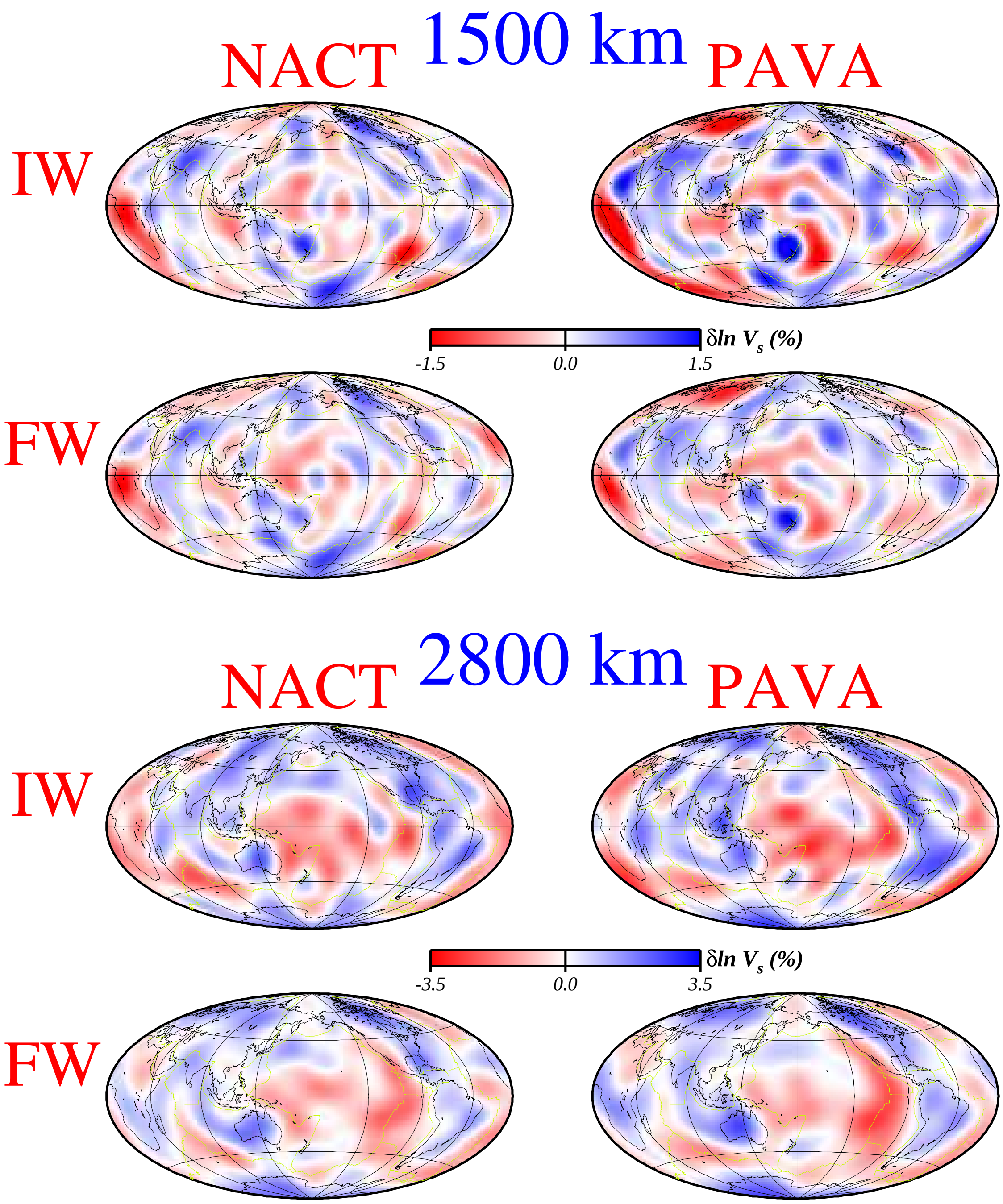
1500 km
NACT
PAVA
IW
FW
δln V_s (%)
-1.5
0.0
1.5
2800 km
NACT
PAVA
IW
FW
δln V_s (%)
-3.5
0.0
3.5

CMB coverage (S_{diff} & ScS)

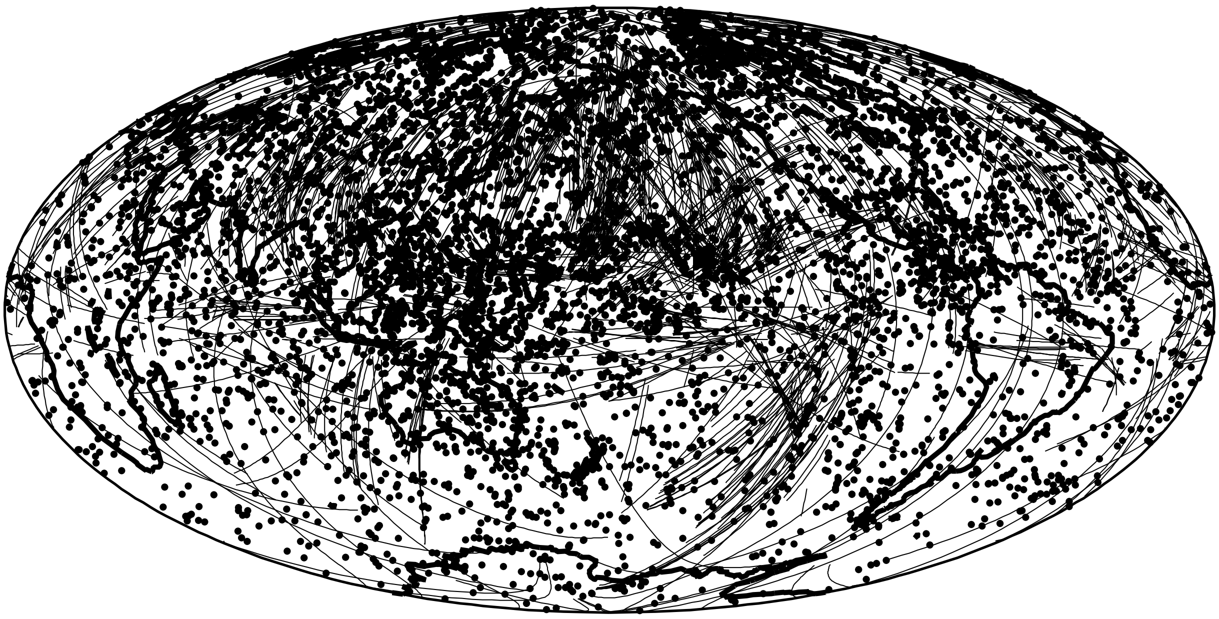

Uppermost mantle-D’’ correlation

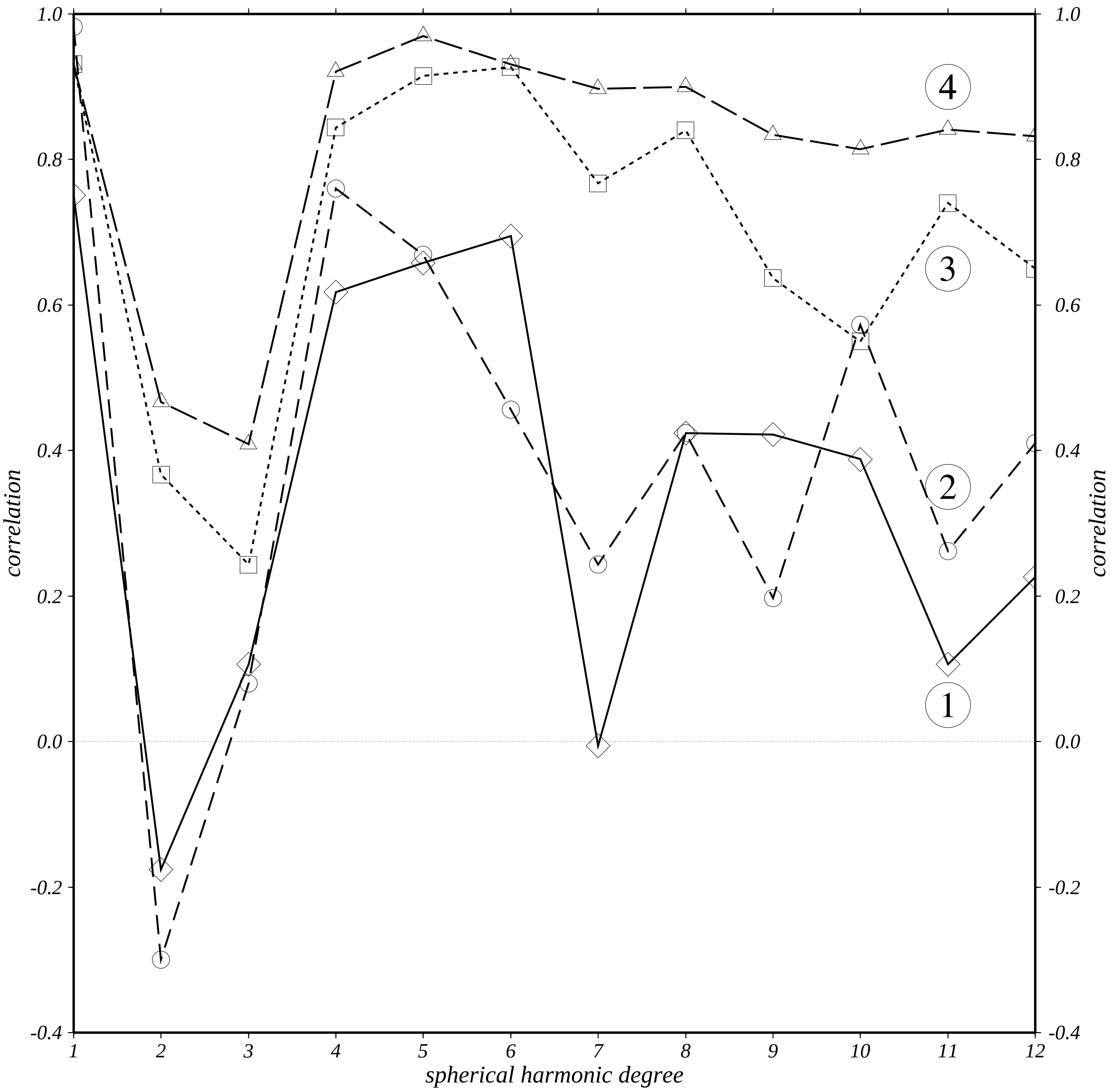

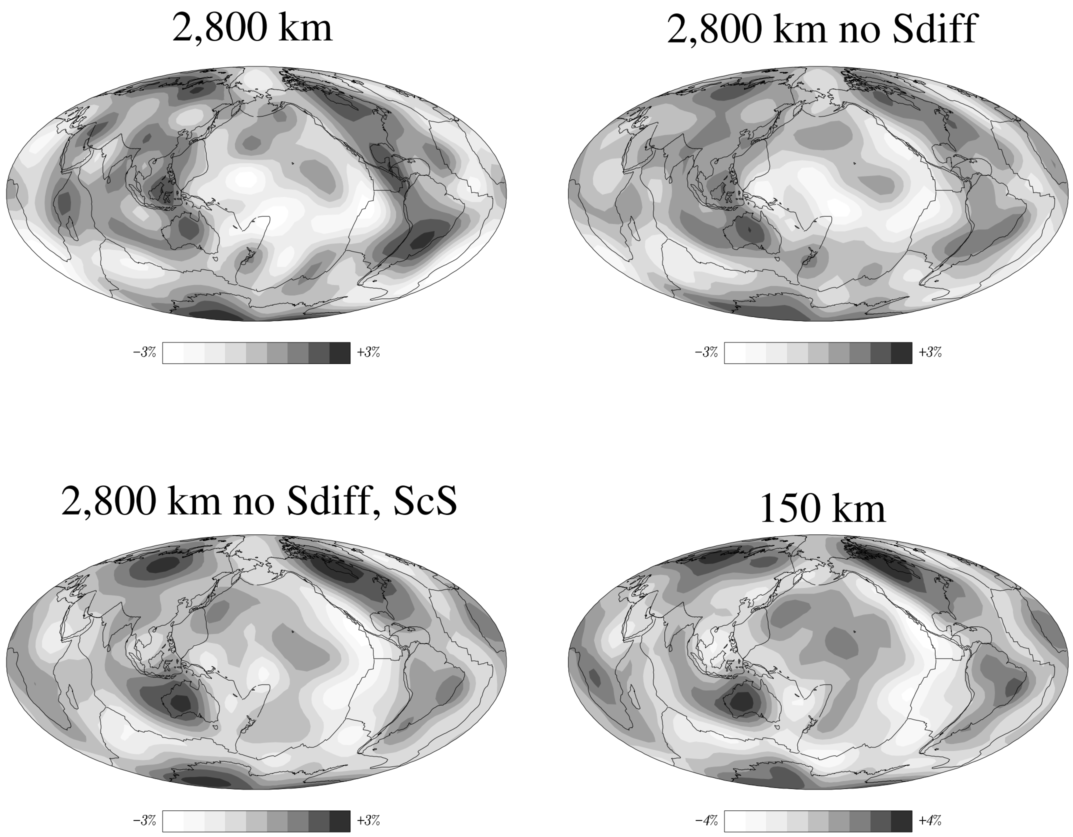
2,800 km
−3%
+3%
2,800 km no Sdiff
−3%
+3%
2,800 km no Sdiff, ScS
−3%
+3%
150 km
−4%
+4%

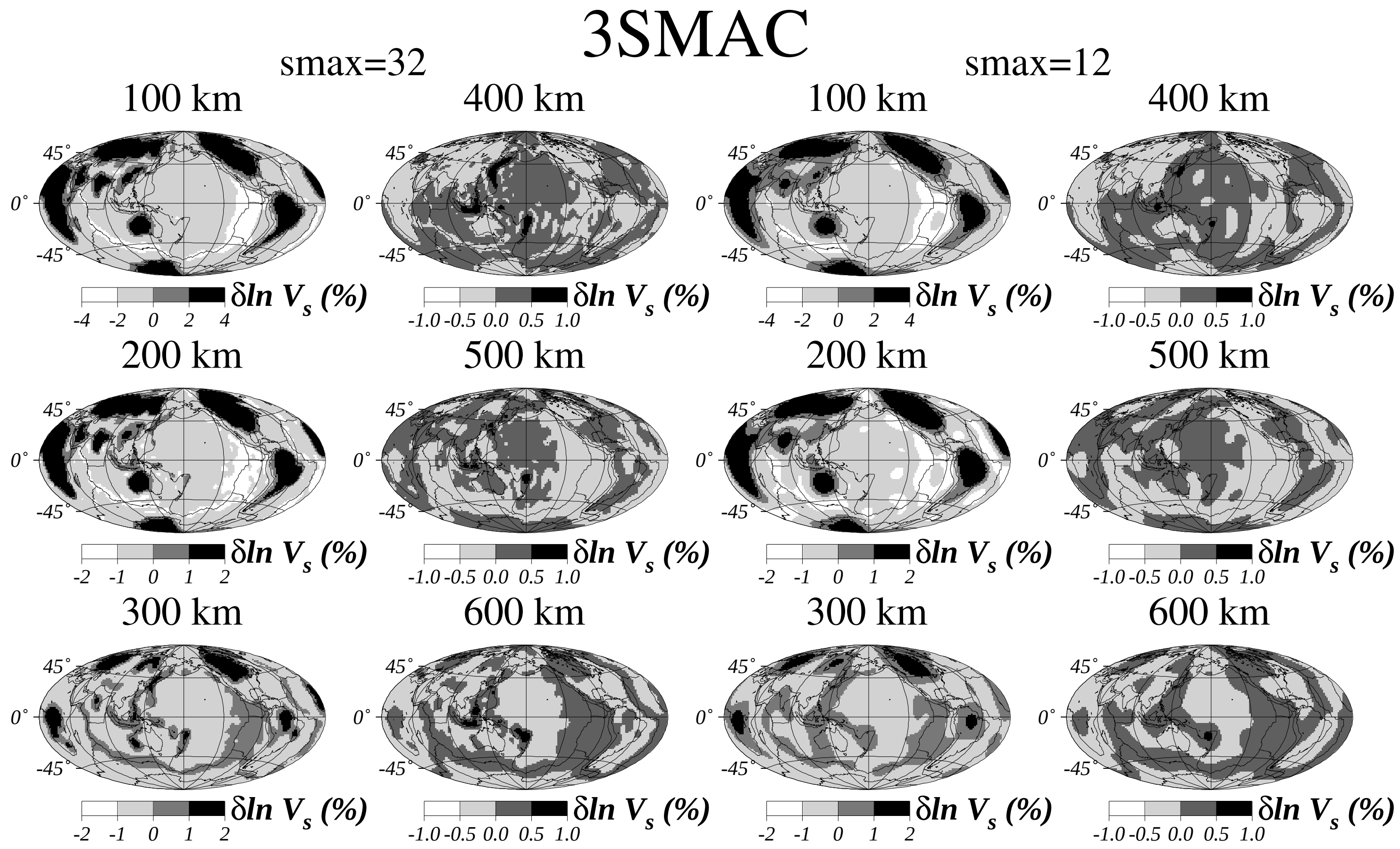

3SMAC
smax=32
smax=12
100 km
400 km
200 km
500 km
300 km
600 km
45°
0°
-45°
δln V_s (%)
-4 -2 0 2 4
-2 -1 0 1 2
-1.0 -0.5 0.0 0.5 1.0

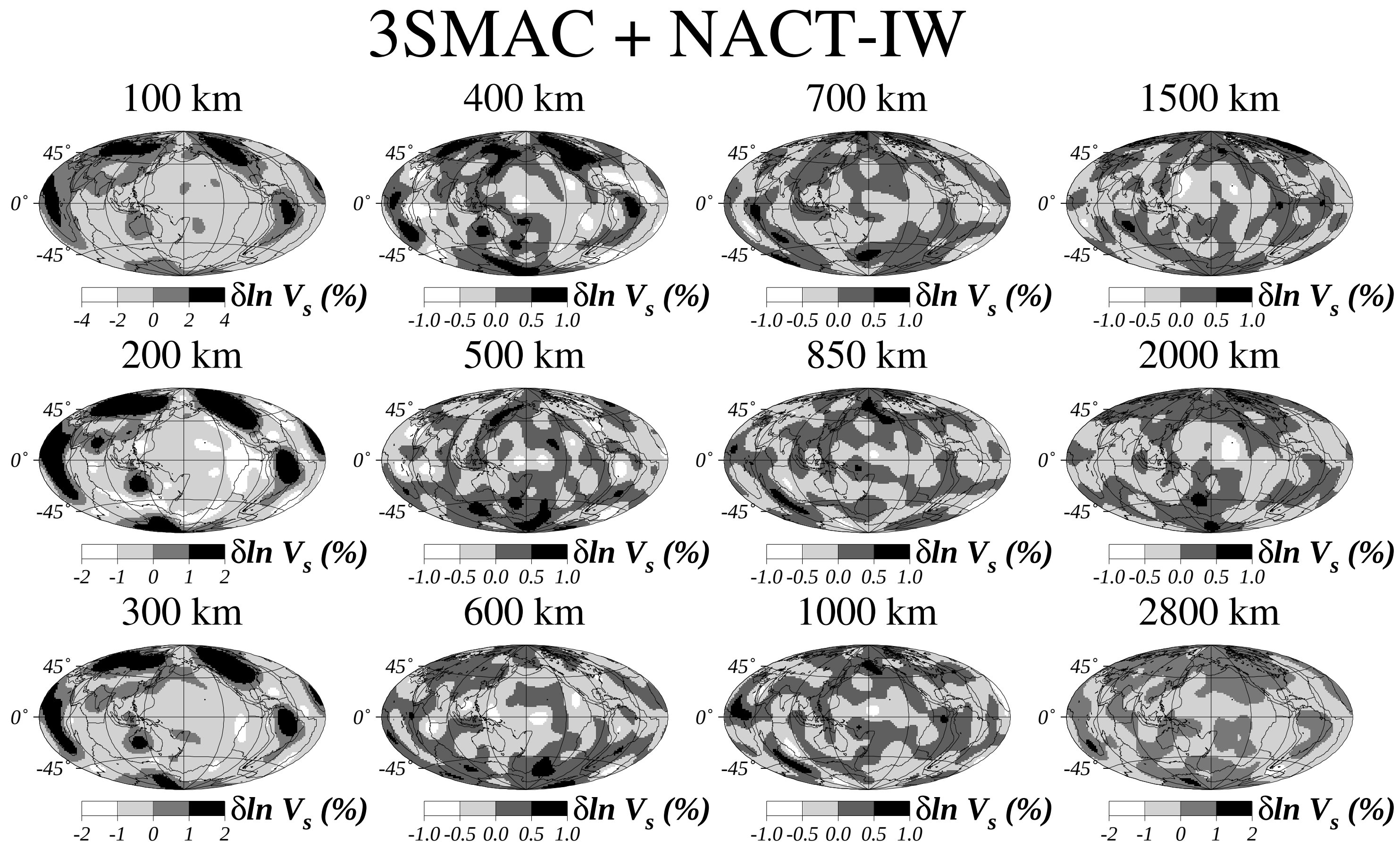
3SMAC + NACT-IW
100 km
400 km
700 km
1500 km
200 km
500 km
850 km
2000 km
300 km
600 km
1000 km
2800 km
45°
0°
-45°
δln Vs (%)
-4 -2 0 2 4
-2 -1 0 1 2
-1.0 -0.5 0.0 0.5 1.0

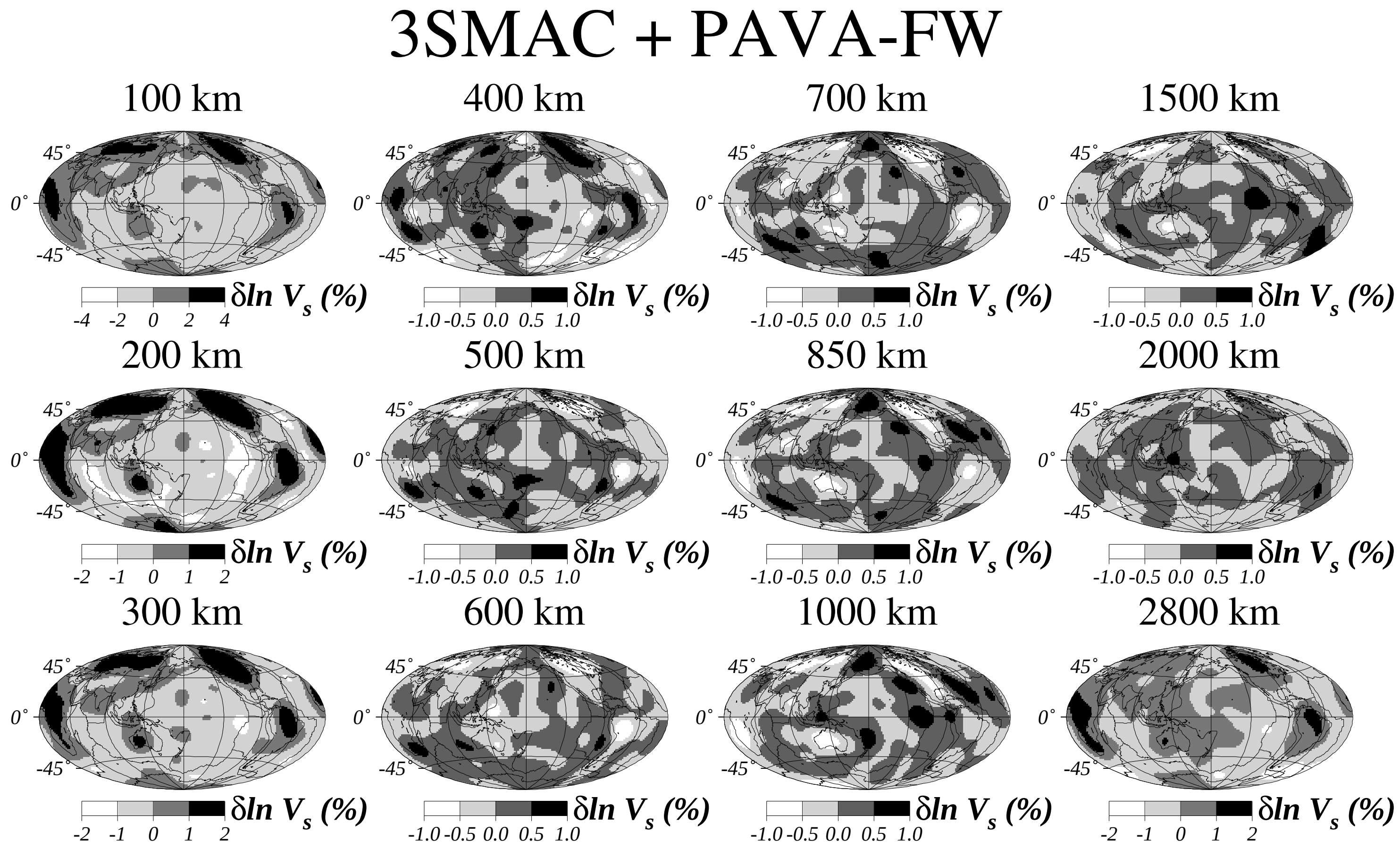
3SMAC + PAVA-FW
100 km
400 km
700 km
1500 km
200 km
500 km
850 km
2000 km
300 km
600 km
1000 km
2800 km
45°
0°
-45°
δln V_s (%)
-4 -2 0 2 4
-2 -1 0 1 2
-1.0 -0.5 0.0 0.5 1.0

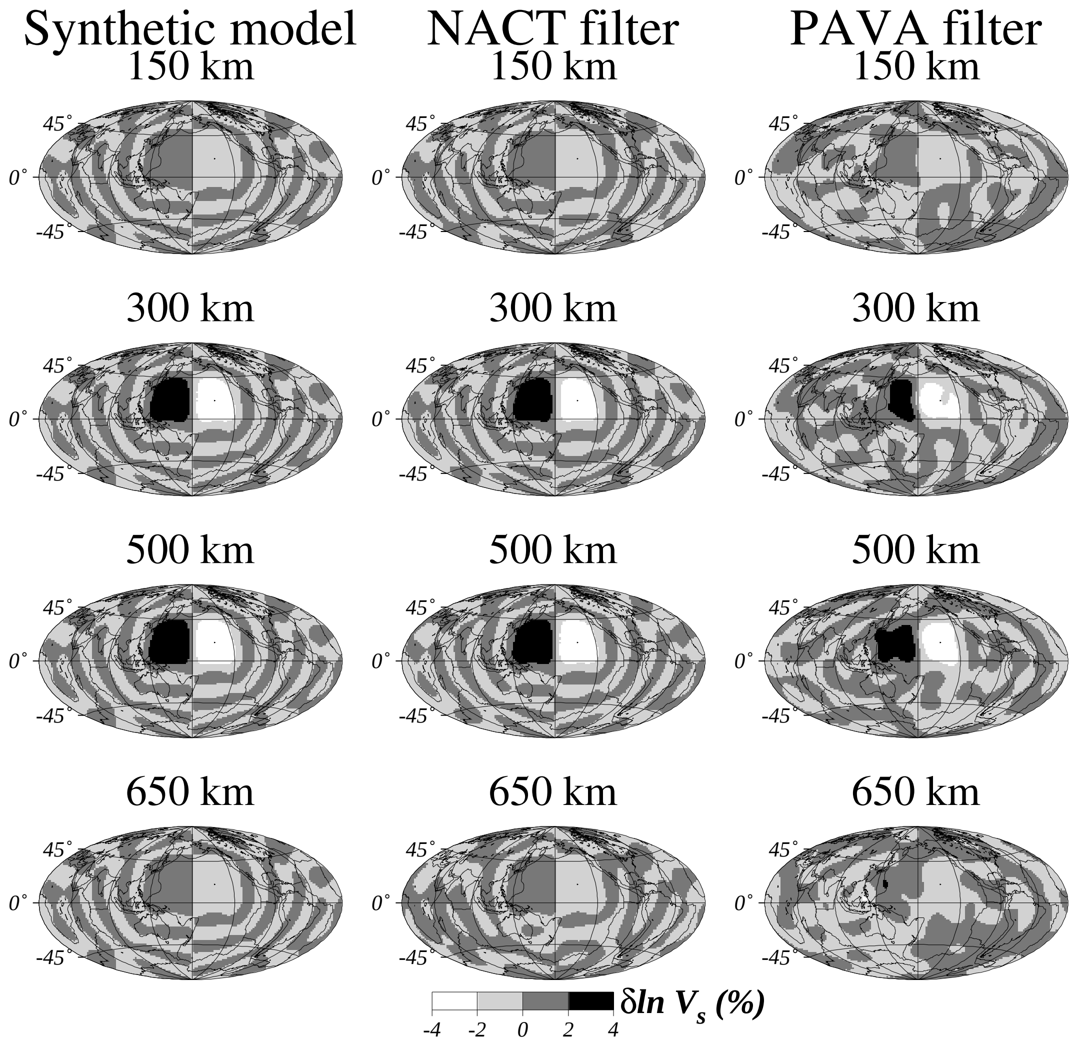
Synthetic model
NACT filter
PAVA filter
150 km
300 km
500 km
650 km
45°
0°
-45°
δln V_s (%)
-4
-2
0
2
4

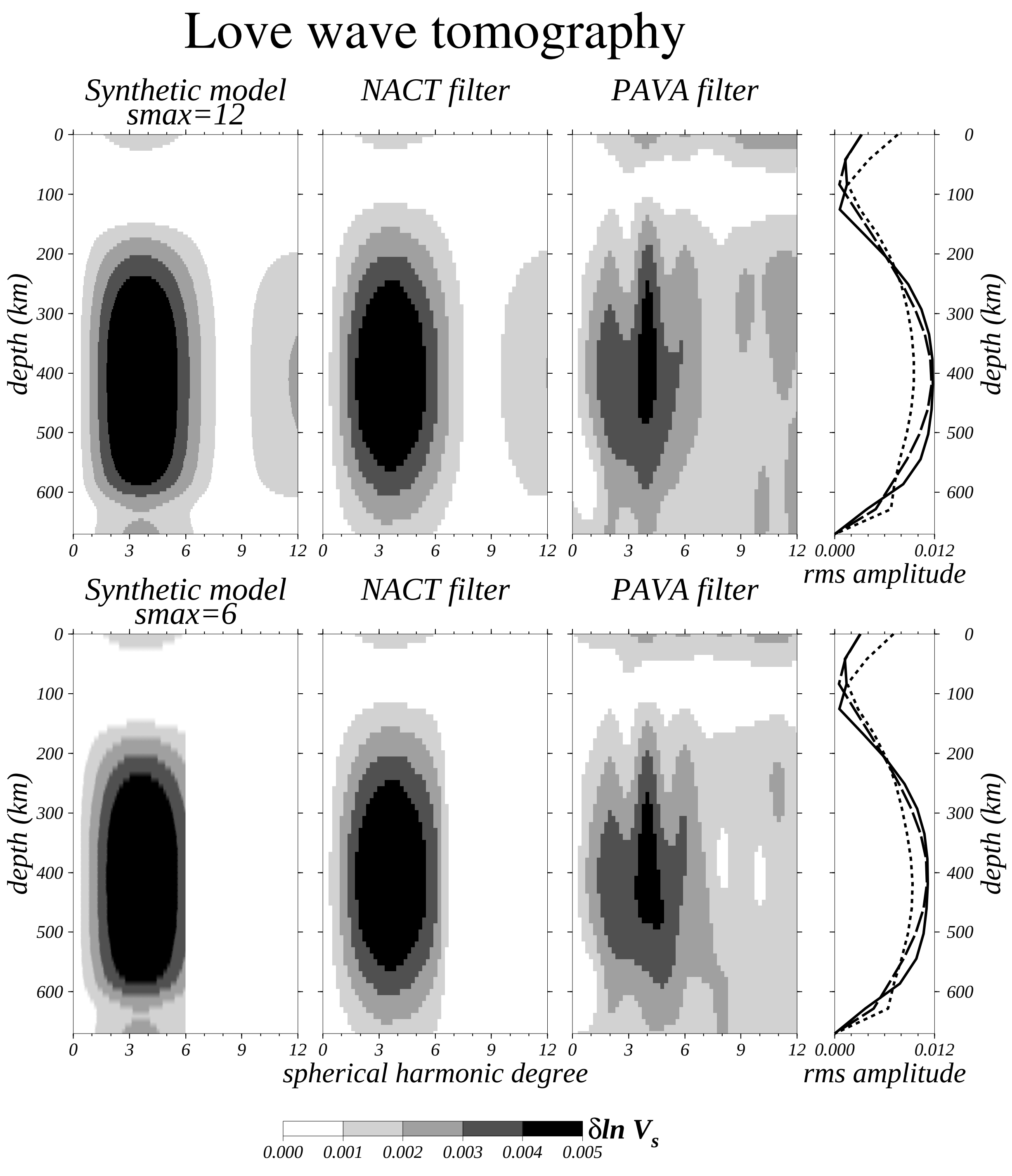
Love wave tomography
Synthetic model smax=12
NACT filter
PAVA filter
Synthetic model smax=6
NACT filter
PAVA filter
depth (km)
0
100
200
300
400
500
600
0 3 6 9 12
spherical harmonic degree
0.000 0.012
rms amplitude
δln V_s
0.000 0.001 0.002 0.003 0.004 0.005